# New SVPWM Used Post a Two-Phase Failure in FOC Five-phase PMSM Drives

Kamel Saleh[a]* and M. Sumner[b]

[a]*Electrical Engineering Dept, An-Najah National University, Nablus, Palestine;*
[b]*Electrical Engineering Dept, Nottingham University, Nottingham, UK*

*kamel.saleh@najah.edu. mark.sumner@nottingham.ac.uk

# New SVPWM Used Post a Two-Phase Failure in FOC Five-phase PMSM Drives

One of the pronounced features of the multi-phase machines compared to the conventional three-phases machine is their high-fault capability. This merit is quite important as it contributes to minimizing the number of interruptions in industrial operations. This paper introduces two new Space Vector Pulse Width Modulation Techniques (SVPWM) to be used with the Field Oriented Control (FOC) strategy under two phases failure of the five-phase motor drives. The first SVPWM technique can be used if the failure happens to the adjacent phases while the second one is used in the cases that the failure happens to non-adjacent phases. The proposed modulation techniques are considering the modifications of the remaining healthy stator currents of the five-phase motor under the failure of the two adjacent phases and non-adjacent phases to maintain the torque producing Magneto Motive Force (MMF) and hence maintain the speed. This will enhance the reliability of the whole drive system. Also, the new SVPWM techniques will reduce the harmonics in the currents and hence reduce the ripple in the torque. Simulation results illustrate the capability of proposed new SVPWM techniques to maintain the torque ripple less than 3.6 % and 3.4% post the failure in adjacent phase and non-adjacent phases respectively.

Keywords: word; five-phase PMSM motor, multi-dimension SVPWM, Asymmtric SVPWM, open-circuit faults

## 2.1 Introduction

Multi-phase motor drives have been received increasing interest in recent years due to many reasons when compared to three-phase motor drives. These reasons are represented in better reliability, efficiency, torque density (Villani, Tursini, Fabri, & Castellini, 2010; Qingguo, Xiaofeng, Fei, & Chengsheng, 2005). Nowadays, many applications are using multi-phase motor drives including electrical vehicles, aerospace, and ships. During the normal operating conditions, multi-dimension SVPWM can be utilized in a multi-phase motor drive to cancel the third harmonic in the stator currents to enhance the torque (Chen, 2015; Xue, Wen, & Feng, 2006; Wang, Zheng, Wu, Zhang, & Li, 2014; Parsa, &

Toliyat, 2007 ).

In the cases of a single-phase failure or two-phase failure of the five-phase motor drive, a fault-tolerant control (FTC) strategy should be adopted to control the current in the healthy phases to ensure a certain optimization criterion including minimum torque ripples, equal phase currents, and minimum copper losses (Bianchi, Bolognani,& Dai Pre, 2007; Mohammadpour, Sadeghi, & Parsa, 2014; Abdel-Khalik, Ahmed, Elserougi, & Massoud, 2015). Traditionally, Most of the AC Drives are using the Phase Voltage Modulation ( PVM ) wither it is sinusoidal PWM (SPVW) or SVPWM under healthy operating condition. This related to the fact that the five phase motors voltage and currents are balanced under healthy operating condition and the PVM techniques are typically for the balanced system. However, if a failure is introduced to the operation of the five-phase motor, the motors voltages and currents become unbalanced and hence, these PVM techniques become likely inapplicable. Thereby in most articles, the hysteresis current controller is utilized to track the currents in the cases of the open-circuit failure in five-phase AC drive system despite the fact that the hysteresis controller may be undesirable in industrial applications due to the inconstant switching frequency (Mohammadpour, Sadeghi, & Parsa, 2014; Abdel-Khalik, Ahmed, Elserougi, & Massoud, 2015; Sedrine, Ojeda, Gabsi, & Slama-Belkhodja, 2015) . For instant (Mohammadpour, Sadeghi, & Parsa, 2014) developed optimal current solutions to enhance the torque ripple for all possible fault conditions of five-phase PMSM. (Sedrine, Ojeda, Gabsi, & Slama-Belkhodja, 2015) enhanced the torque ripple for a flux-switching motor having a small mutual-inductance by using genetic algorithm to obtain optimal current solution. However, these techniques are dependent on motor parameters in addition to the use of the hysteresis control to track the current trajectory. To avoid using hysteresis control (Liu, Qu, Zhao, Chen, & Xie, 2016) presented two SVPWM strategies for a five-phase

motor under a failure in one phase. But, this techniques are not applicable if two phase of the five-phase motor are failure in addition to the fact theses techniques are tested at low speeds only. (Chen, Liu, Zhao, Qu, & Xu, 2017), developed an asymmetrical SVWPM for five phase motors under a single-phase open circuit. The presented technique is not applicable in the cases when the failure is in two phases.

The implementation of Vector Control (VC) of five-phase motor in the cases of a failure in one phase is introduced by (Guzman, Duran, Barrero, Zarri, Bogado, Prieto, & Arahal, 2016; Cheng, Sui, Zheng, Wang, & Wu, 2018) and (Zhou, Zhao, Liu, Cheng, & Xie, 2017; Chen, Zhao, Liu, & Lin, 2019; Chen, Gu, Lin, & Liu, 2020) through presenting the reduced-order transformation matrices and the reduced-order orthogonal transformation respectively. However, these techniques are not applicable in the case when the failure are in two phases. (Tian et al 2017) proposed a reduced-order non-orthogonal transformation matrices in five-phase PM motor in the case when the failure is in two phases. (Bermudez, Gonzalez-Prieto, Barrero, Guzman, Kestelyn, & Duran 2018) presented a virtual vector-based direct-torque-control (DTC) for a 5Ph induction motor under open faults. (Tian, Mirzaeva, An, Sun, & Semenov, 2018), proposed a sliding mode control to control the d-q frame current. Recently, (Huang, Hua, Chen, Yin, & Qi, 2018), introduced a model predictive control to enhance the torque ripple through the third harmonic injection.

FOC under single-phase failure of five-phase motor using d-q frame and PWM techniques was introduced by (Priestley, Farshadnia, & Fletcher, 2019). This technique is less parameter-dependent than the model-based methods. Similar work is done by (Tian, et al 2019) but by using a well-decoupled model. Despite several other papers that are investigating the SVPWM of 5Ph drives under a failure in one phase, a feasible PWM technique under two-phase open faults is rarely reported.

This paper introduces two novel SVPWM techniques that can be used in the Field Oriented Control (FOC) of the five-phase motor drive in cases of two-phase failure in the adjacent and the non-adjacent phases respectively. The proposed modulation techniques are developed according to the reconstructed space vector diagrams. The reconstructed space vector diagrams reflect the change in magnitudes and phases of the remaining healthy stator currents of the five-phase motor under the faults to maintain the torque producing Magneto Motive Force (MMF) and hence maintain the speed. This will enhance the reliability of the whole drive system and results in minor system performance degradation under the two-phase failure. The new technique is simple to implement in hardware compared to other techniques and need no extra memory. Also it is using FOC control which widely used in industry. Most importantly, it very suitable to be implemented in the cases when the sensorless control of the five phase motor using the fundamental PWM excitation method under the two phases failure is wanted. One of the challenges that faces this technique and that should be further investigated in future is the switching losses associated with the new technique. It is well known that the SVPWM increases the switching losses due to the existence of the third harmonic compared to the SPWM. Under healthy operating conditions the third harmonics is cancelled through third harmonic injection. While in the case of two-phase failure, the third harmonic is still there due to the unapplicable of the harmonic injection and so the switching losses is expected to increase.

### 2.1 *Five-phase PMSM drive*

Figure 1 illustrates the five-phase PMSM drive topology (Hyung-Min, Ji-Woong, & Seung-Ki, 2004). The PMSM motor is modeled according to equations (1--5).

$$\begin{bmatrix} \mathrm{v}_a \\ \mathrm{v}_b \\ \mathrm{v}_c \\ \mathrm{v}_d \\ \mathrm{v}_e \end{bmatrix} = r_s * \begin{bmatrix} i_a \\ i_b \\ i_c \\ i_d \\ i_e \end{bmatrix} + \begin{bmatrix} d\emptyset_a/dt \\ d\emptyset_b/dt \\ d\emptyset_c/dt \\ d\emptyset_d/dt \\ d\emptyset_e/dt \end{bmatrix} \quad (1)$$

$$\begin{bmatrix} \emptyset_a \\ \emptyset_b \\ \emptyset_c \\ \emptyset_d \\ \emptyset_e \end{bmatrix} = \begin{bmatrix} L_{aa} L_{ab} L_{ac} L_{ad} L_{ae} \\ L_{ab} L_{bb} L_{bc} L_{bd} L_{be} \\ L_{ac} L_{bc} L_{cc} L_{cd} L_{ce} \\ L_{ad} L_{bd} L_{cd} L_{dd} L_{de} \\ L_{ae} L_{be} L_{ce} L_{de} L_{ee} \end{bmatrix} \begin{bmatrix} i_a \\ i_b \\ i_c \\ i_d \\ i_e \end{bmatrix} + \begin{bmatrix} \varphi_{ma} \\ \varphi_{mb} \\ \varphi_{mc} \\ \varphi_{md} \\ \varphi_{me} \end{bmatrix} \quad (2)$$

Where $\mathrm{v}_{a,b,c,d,e}$ are the stator voltages, $r_s$ is the stator resistance, $i_{a,b,c,d,e}$ are the stator currents , $\emptyset_{a,b,c,d,e}$ are the stator linking fluxes, $L_{aa}$, $L_{bb}$, $L_{cc}$, $L_{dd}$ and $L_{ee}$ are the total stator self-inductances, and $L_{ab}$, $L_{ac}$ , $L_{ba}$ , $L_{ad}$, $L_{ae}$, $L_{bc}$ , $L_{bd}$ , $L_{be}$ , $L_{cd}$ , $L_{ce}$ and $L_{de}$ are the total stator mutual inductances. $\varphi_{ma,b,c,d,e}$ are the permanent magnet fluxes.

The stator total self and mutual inductances are dependent on rotor angle as shown below:-

$$\begin{bmatrix} L_{aa} \\ L_{bb} \\ L_{cc} \\ L_{dd} \\ L_{ee} \end{bmatrix} = \begin{bmatrix} L_{so} + L_{sl} \\ L_{so} + L_{sl} \\ L_{so} + L_{sl} \\ L_{so} + L_{sl} \\ L_{so} + L_{sl} \end{bmatrix} + L_x * \begin{bmatrix} cos(2\theta_r) \\ cos(2\theta_r - 2\theta_x) \\ cos(2\theta_r - 4\theta_x) \\ cos(2\theta_r - 6\theta_x) \\ cos(2\theta_r - 8\theta_x) \end{bmatrix} (3),$$

$$\begin{bmatrix} L_{ab} \\ L_{ac} \\ L_{ad} \\ L_{ae} \\ L_{bc} \\ L_{bd} \\ L_{be} \\ L_{cd} \\ L_{ce} \\ L_{de} \end{bmatrix} = L_{so} * \begin{bmatrix} \cos(2\theta_x) \\ \cos(4\theta_x) \\ \cos(6\theta_x) \\ \cos(8\theta_x) \\ \cos(2\theta_x) \\ cos(4\theta_x) \\ cos(4\theta_x) \\ cos(2\theta_x) \\ cos(4\theta_x) \\ \cos(2\theta_x) \end{bmatrix} + L_x * \begin{bmatrix} \cos(2\theta_r - 2\theta_x) \\ \cos(2\theta_r - 4\theta_x) \\ \cos(2\theta_r - 6\theta_x) \\ \cos(2\theta_r + 8\theta_x) \\ \cos(2\theta_r - 6\theta_x) \\ cos(2\theta_r - 8\theta_x) \\ cos(2\theta_r) \\ cos(2\theta_r) \\ cos(2\theta_r - 2\theta_x) \\ \cos(2\theta_r - 4\theta_x) \end{bmatrix} (4)$$

where: $L_{so}$ and , $L_{sl}$ is the stator mutual and self inductance. $L_x$ is the stator inductance fluctuation, and $\theta_x \, is \, \pi/5$. both stator self and mutual inductance are modulated by saturation saliency that appears in the term $(2\theta_r)$.

The stator flux-linkages due to the permanent magnet are

$$\begin{bmatrix} \varphi_{ma} \\ \varphi_{mb} \\ \varphi_{mc} \\ \varphi_{md} \\ \varphi_{me} \end{bmatrix} = \Lambda_m * \begin{bmatrix} cos(\theta_r) \\ cos(\theta_r - 2\theta_x) \\ cos(\theta_r - 4\theta_x) \\ cos(\theta_r - 6\theta_x) \\ cos(\theta_r - 8\theta_x) \end{bmatrix} (5),$$

where $\Lambda_m$ is the peak permanent magnet flux linkage.

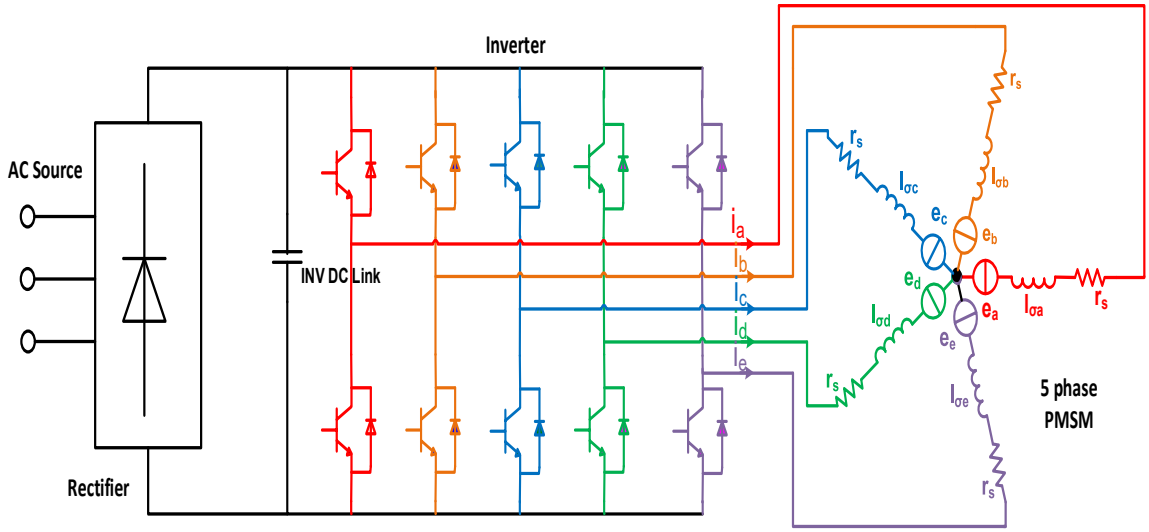


Figure 1. Five-phase PMSM Drive.

### *2.2 Currents of the five-phase motor post the failure.*

Five-phase motor drives are potentially fault-tolerant as mentioned previously. By utilizing a proper fault-tolerant control technique, the five-phase motor can maintain performance even post a two-phase failure. The fault-tolerant control technique should maintain the torque-producing MMF without the need to use a neutral line to ensure safe operation.

Now, if five sinusoidal currents shifted by $2\pi/5$ degrees are passing through five stator windings distributed sinusoidally, then the stator phases MMFs are given as

follows (Parsa, & Toliyat, 2007; Fu, & Lipo, 1994; Zhang, Xu,Enjeti, Li, Hawke, & Krishnamoorthy,2014; Tani, Mengoni, Zarri, Serra & Casadei, 2012):

$$MMF_a(\emptyset,\theta) = \frac{N_s}{2} I_m \cos(\emptyset)\cos(\theta_r) \quad (6)$$

$$MMF_b(\emptyset,\theta) = \frac{N_s}{2} I_m \cos(\emptyset - 2\theta_x)\cos(\theta_r - 2\theta_x) \quad (7)$$

$$MMF_c(\emptyset,\theta) = \frac{N_s}{2} I_m \cos(\emptyset - 4\theta_x)\cos(\theta_r - 4\theta_x) \quad (8)$$

$$MMF_d(\emptyset,\theta) = \frac{N_s}{2} I_m \cos(\emptyset + 4\theta_x)\cos(\theta_r + 4\theta_x) \quad (9)$$

$$MMF_e(\emptyset,\theta) = \frac{N_s}{2} I_m \cos(\emptyset + 2\theta_x)\cos(\theta_r + 2\theta_x) \quad (10)$$

Where $N_s$ is the total number of turns for each phase, $\emptyset$ is the spatial angle, and $\theta_r = \omega t$. $I_m$ is the amplitude of the phase current. The stator total MMF is the sum of the MMF of all the phases, i.e.

$$MMF_t(\emptyset,\theta_r) = MMF_a(\emptyset,\theta_r) + MMF_b(\emptyset,\theta_r) + MMF_c(\emptyset,\theta_r) + MMF_d(\emptyset,\theta_r) + MMF_e(\emptyset,\theta_r) \quad (11)$$

Which yields :-

$$MMF_t(\emptyset,\theta_r) = \frac{5}{4}(N_s I_m \cos(\theta_r - \emptyset)) \quad (12)$$

Equation 12 can be rewritten as:-

$$MMF_t(\emptyset,\theta) = \frac{5}{8}(N_s I_m(e^{j\theta_r}e^{-j\emptyset} + e^{-j\theta_r}e^{j\emptyset}) \quad (13)$$

The total MMF can be also written as:-

$$MMF_t = \frac{1}{4}\{N_s[(i_a + e^{-2j\theta_x} i_b + e^{-4j\theta_x} i_c + e^{4j\theta_x} i_d + e^{2j\theta_x} i_e)e^{\emptyset} + (i_a + e^{2j\theta_x} i_b + e^{4j\theta_x} i_c + e^{-4j\theta_x} i_d + e^{-2j\theta_x} i_e)e^{-\emptyset}]\} \quad (14)$$

Combining 13 and 14 yields:-

$$\frac{5}{2} I_m e^{j\theta} = i_a + e^{2j\theta_x} i_b + e^{4j\theta_x} i_c + e^{-4j\theta_x} i_d + e^{-2j\theta_x} i_e \quad (15)$$

$$= \begin{bmatrix} I_m * \cos(wt) \\ I_m * \cos(wt - 2\theta_x) \\ I_m * \cos(wt - 4\theta_x) \\ I_m * \cos(wt + 4\theta_x) \\ I_m * \cos(wt + 2\theta_x) \end{bmatrix} \quad (16)$$

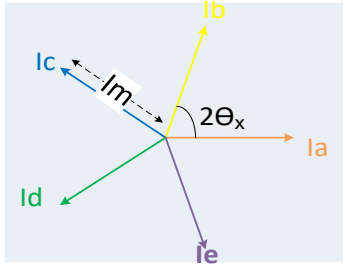


Figure 2 healthy distribution of stator currents.

If failure is introduced to phase 'a' as an example, The MMF can be maintained by setting the current in phase 'a' to zero in equation (15) and assuming that :

$$i'_b = -i'_d \ , i'_c = -i'_e \quad (17)$$

Where $i'_b$ , $i'_c$ , $i'_d$ , and $i'_e$ are the remaining stator currents post the failure in phase 'a'.

The currents in the remaining phases are found to be:-

$$i'_b = -i'_d \ = \frac{5I_m}{4(sin(\theta_x))^2} cos(\theta_r - \theta_x) \ , i'_c = -i'_e \ = \frac{5I_m}{4(sin(\theta_x))^2} cos(\theta_r - 4\theta_x) \ (18)$$

Which means that to maintain the MMF distribution in case of a failure in one phase in five-phase motor drive, the stator currents in the remaining healthy phases should be to be increased by 138.2% compared to its value under the healthy condition as shown in equation 19 and figure 3. Also, the currents in the phase besides the faulted phase should be shifted by $(\pi/5)$ towards the faulted phase.

$$\begin{bmatrix} I'_a \\ I'_b \\ I'_c \\ I'_d \\ I'_e \end{bmatrix} = \begin{bmatrix} 0 \\ 1.382 * I_m * \cos(wt - \theta_x) \\ 1.382 * I_m * \cos(wt - 4\theta_x) \\ 1.382 * I_m * \cos(wt - 6\theta_x) \\ 1.382 * I_m * \cos(wt - 9\theta_x) \end{bmatrix} \quad (19)$$

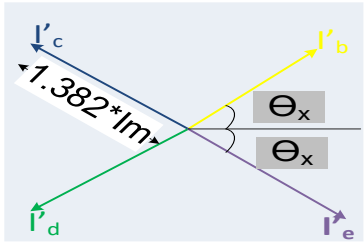


Figure 3 distribution of stator currents post a failure in phase 'a'.

In the same way, when the adjacent phases 'a' and 'b' are exposed to a failure, the MMF

can be maintained assuming that the sum of remaining currents should be zero as follows:-

$$i_c'' = \frac{5I_m \cos(\theta_x)}{2(\sin(2\theta_x))^2}\cos(\theta_r - 2\theta_x), i_d'' = \frac{5I_m \cos(\theta_x)^2}{(\sin(2\theta_x))^2}\cos(\theta_r - 4\theta_x), i_e''$$

$$= \frac{5I_m \cos(\theta_x)}{2(\sin(2\theta_x))^2}\cos(\theta_r) \quad (20)$$

Where $i_c''$ , $i_d''$ , and $i_e''$ are the remaining stator currents post the failure in the adjacent phases ‘a’ and ‘b’.

The distribution of the stator currents post the failure in the adjacent phases “a” and “b” is shown in equation 21 and figure 4.

$$\begin{bmatrix} I''_a \\ I''_b \\ I''_c \\ I''_d \\ I''e \end{bmatrix} = \begin{bmatrix} 0 \\ 0 \\ 2.236 * I_m * \cos(wt - 2\theta_x) \\ 3.618 * I_m * \cos(wt + 4\theta_x) \\ 2.236 * I_m * \cos(wt) \end{bmatrix} \quad (21)$$

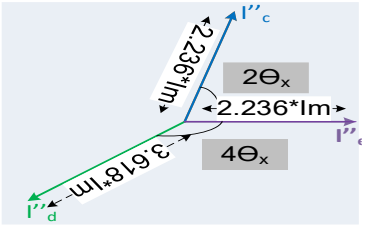


Figure 4 distribution stator current post the failure in two adjacent phases ’a’ and ‘b’ .

Finally, if the failure is introduced to the non-adjacent phases ‘b’ and ‘e’, the MMF can be maintained assuming that the sum of remaining currents should be zero as follows:-

$$i_a'' = \frac{5I_m}{4(\sin(2\theta_x))^2}\cos(\theta_r), i_c'' = \frac{5I_m}{8(\sin(2\theta_x))^2\cos(3\theta_x)}\cos(\theta_r - 3\theta_x), i_d''$$

$$= \frac{5I_m}{8(\sin(2\theta_x))^2\cos(2\theta_x)}\cos(\theta_r + 3\theta_x) \quad (22)$$

The distribution of the stator currents post failure in the non-adjacent phases “b” and “e” are is shown in equation 23 and figure 4.

$$\begin{bmatrix} I''_a \\ I''_b \\ I''_c \\ I''_d \\ I''e \end{bmatrix} = \begin{bmatrix} 1.382 * I_m * \cos(wt) \\ 0 \\ 2.236 * I_m * \cos(wt - 3\theta_x) \\ 2.236 * I_m * \cos(wt - 3\theta_x) \\ 0 \end{bmatrix} \quad (23)$$

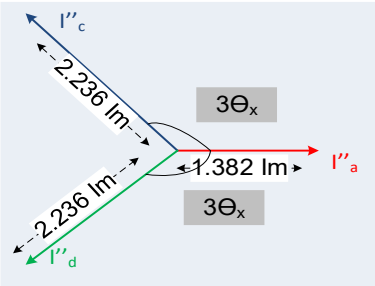


Figure 5 distribution stator current post the failure in the non-adjacent phases 'b' and e'.

### *2.2 SVPWM of the Fault -Tolerant PMSM*

#### *2.3.1 SVPWM under healthy operating condition*

To regulate the currents according to equation (15), multi-Dimension SVPWM can be used (Chen, 2015; Xue, Wen, & Feng, 2006; Wang, Zheng, Wu, Zhang, & Li, 2014; Parsa, & Toliyat, 2007). In this method, the fundamental component of the reference voltage (V_ref) is mapped into α1-β1 stationary frame and the third harmonic frame of the reference voltage will be mapped into α3-β3 stationary frame as shown in Figure 6.

The amplitude of the vectors are as follows: minimum vector(Vmin)=0.2472VDC, medium vectors(Vmid)=0.4VDC, and maximum vectors(Vmax)=0.6472VDC.

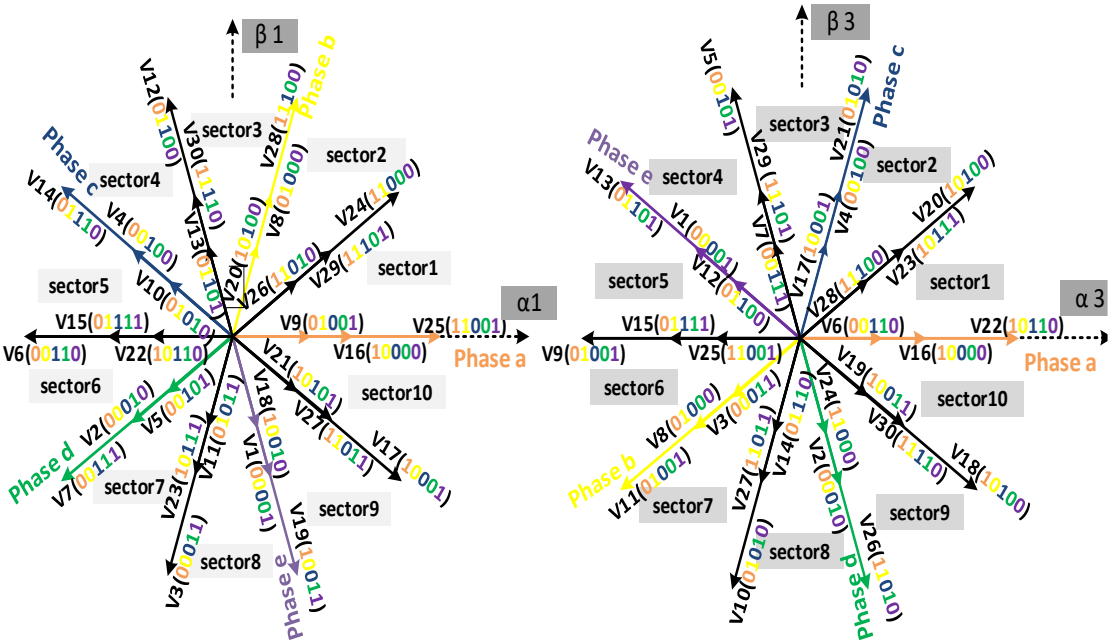


Figure 6. switching vectors on α1 –β1 plane and α3 –β3 plane in multi-dimension SVPWM.

The algorithm to implement the multi-Dimension SVPWM is shown in figure 7. A fast preview of the working of each block will be presented here

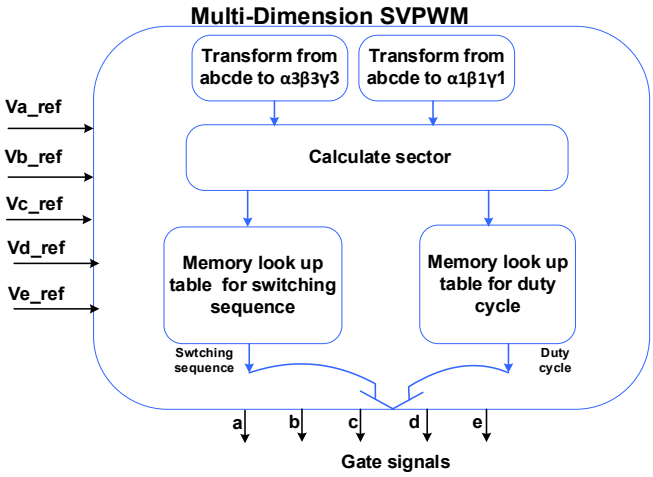


Figure 7. The algorithm of the multi-dimension SVPWM

Firstly, the sector where the reference voltage (V_ref) is located can be identified according to equation (24). and table 1.

$$\theta = \arctan\left(\frac{V\_ref\beta 1}{V\_ref\alpha 1}\right) \qquad (24)$$

**Table 1.** Selection of the Sector in multi-Dimension SVPWM .

| Angle of reference voltage (θ) | Sector number |
|---|---|
| $0 \le \theta < \theta_x$ | 1 |
| $\theta_x \le \theta < 2\theta_x$ | 2 |
| $2\theta_x \le \theta < 3\theta_x$ | 3 |
| $3\theta_x \le \theta < 4\theta_x$ | 4 |
| $4\theta_x \le \theta < 5\theta_x$ | 5 |
| $5\theta_x \le \theta < 6\theta_x$ | 6 |
| $6\theta_x \le \theta < 7\theta_x$ | 7 |
| $7\theta_x \le \theta < 8\theta_x$ | 8 |
| $8\theta_x \le \theta < 9\theta_x$ | 9 |
| $9\theta_x \le \theta < 10\theta_x$ | 10 |

Secondly, the dwell time is calculated as shown in figure 8 and the equations below. Figure 8 illustrates how the adjacent active vectors (V16=10000, V24= 11000, V25=11001 , and V29=11101) in addition to the two null vectors (V0=00000, V32=11111) are utilized to generate the reference voltage (V_ref) which exists in the first sector. The time duration of applying the vectors V16,V24,V25,V29 and V0 i.e (T1,T2,T3,T4 and T0) can be obtained as follows :-

$$\begin{bmatrix} T_1 \\ T_2 \\ T_3 \\ T_4 \end{bmatrix} = Ts \times [T^{-1}] \begin{bmatrix} \mathrm{V\_ref\_}\,\alpha 1 \\ \mathrm{V\_ref\_}\,\beta 1 \\ \mathrm{V\_ref\_}\,\alpha 3 \\ \mathrm{V\_ref\_}\,\beta 3 \end{bmatrix} (25)\ ,$$

$$\mathrm{T} = \begin{bmatrix} V_{mid} & V_{max}\cos(2\theta_x) & V_{max} & V_{mid}\cos(2\theta_x) \\ 0 & V_{max}\sin\ (2\theta_x) & 0 & V_{mid}\sin\ (2\theta_x) \\ V_{mid} & V_{min}\cos(8\theta_x) & -V_{min} & V_{mid}\cos(3\theta_x) \\ 0 & V_{min}\sin\ (8\theta_x) & 0 & V_{mid}\sin\ (3\theta_x) \end{bmatrix} (26)$$

$$T_0 = T_s - T_1 - T_2 - T_3 - T_4 \ \ (27)\ ,$$

Where Ts is the sampling time.

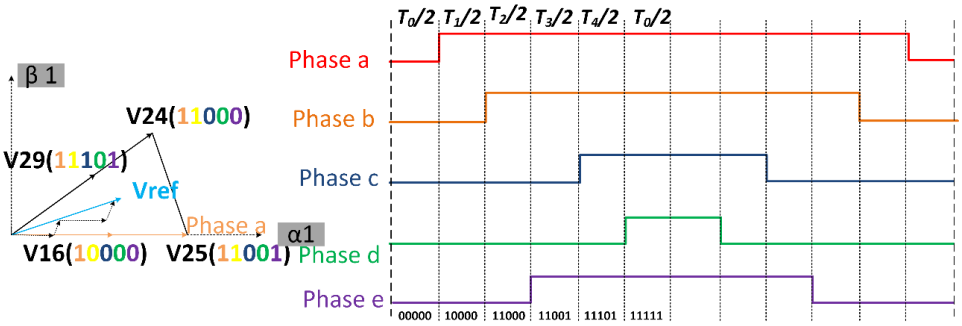


Figure 8. illustration of the vectors and the switching sequence used to generate the reference voltage vector located in the first sector using multi-dimension SVPWM.

Finally, The dwell time in other sectors and the correct switching sequence are given in table 2.

Table 2: Dwell time calculation and switching sequence in multi-Dimension SVPWM

| Dwell Time | Switching sequency |
|---|---|
| $\begin{bmatrix}T1\\T2\\T3\\T4\end{bmatrix} = \begin{bmatrix}0.6910 & -0.9511 & 1.8090 & 0.5878\\ 0 & 1.9021 & 0 & -1.1756\\ 1.1180 & -1.5388 & -1.1180 & -0.3633\\ 0 & 1.1756 & 0 & 1.9021\end{bmatrix} * \begin{bmatrix}v\alpha1\\v\beta1\\v\alpha3\\v\beta3\end{bmatrix} * (\frac{Ts}{VDC})$ | $V16, V24, V25, V29$ |
| $\begin{bmatrix}T1\\T2\\T3\\T4\end{bmatrix} = \begin{bmatrix}-0.6910 & 0.9511 & -1.8090 & -0.5878\\ 1.8090 & -0.5878 & 0.6910 & -0.9511\\ -1.1180 & 1.5388 & 1.1180 & 0.3633\\ 1.1180 & -0.3633 & -1.1180 & 1.5388\end{bmatrix} * \begin{bmatrix}v\alpha1\\v\beta1\\v\alpha3\\v\beta3\end{bmatrix} * (\frac{Ts}{VDC})$ | $V8, V24, V28, V29$ |
| $\begin{bmatrix}T1\\T2\\T3\\T4\end{bmatrix} = \begin{bmatrix}1.1180 & 0.3633 & -1.1180 & -1.5388\\ -1.8090 & 0.5878 & -0.6910 & 0.9511\\ 1.8090 & 0.5878 & 0.6910 & 0.9511\\ -1.1180 & 0.3633 & 1.1180 & 1.5388\end{bmatrix} * \begin{bmatrix}v\alpha1\\v\beta1\\v\alpha3\\v\beta3\end{bmatrix} * (\frac{Ts}{VDC})$ | $V8, V12, V28, V30$ |
| $\begin{bmatrix}T1\\T2\\T3\\T4\end{bmatrix} = \begin{bmatrix}-1.1180 & -0.3633 & 1.1180 & 1.5388\\ 1.1180 & 1.5388 & -1.1180 & 0.3633\\ -1.8090 & -0.5878 & -0.6910 & -0.9511\\ 0.6910 & 0.9511 & 1.8090 & -0.5878\end{bmatrix} * \begin{bmatrix}v\alpha1\\v\beta1\\v\alpha3\\v\beta3\end{bmatrix} * (\frac{Ts}{VDC})$ | $V4, V12, V14, V30$ |
| $\begin{bmatrix}T1\\T2\\T3\\T4\end{bmatrix} = \begin{bmatrix}0 & 1.1756 & 0 & 1.9021\\ -1.1180 & -1.5388 & 1.1180 & -0.3633\\ 0 & 1.9021 & 0 & -1.1756\\ -0.6910 & -0.9511 & -1.8090 & 0.5878\end{bmatrix} * \begin{bmatrix}v\alpha1\\v\beta1\\v\alpha3\\v\beta3\end{bmatrix} * (\frac{Ts}{VDC})$ | $V4, V6, V14, V15$ |

| | |
|---|---|
| $\begin{bmatrix} T1 \\ T2 \\ T3 \\ T4 \end{bmatrix} = \begin{bmatrix} -0.6910 & 0.9511 & -1.8090 & -0.5878 \\ 0 & -1.9021 & 0 & 1.1756 \\ -1.1180 & 1.5388 & 1.1180 & 0.3633 \\ 0 & -1.1756 & 0 & -1.9021 \end{bmatrix} * \begin{bmatrix} v\alpha 1 \\ v\beta 1 \\ v\alpha 3 \\ v\beta 3 \end{bmatrix} * (\frac{Ts}{VDC})$ | $V2, V6, V7, V15$ |
| $\begin{bmatrix} T1 \\ T2 \\ T3 \\ T4 \end{bmatrix} = \begin{bmatrix} -1.1180 & 0.3633 & 1.1180 & -1.5388 \\ 1.1180 & -1.5388 & -1.1180 & -0.3633 \\ -1.8090 & 0.5878 & -0.6910 & 0.9511 \\ 0.6910 & -0.9511 & 1.8090 & 0.5878 \end{bmatrix} * \begin{bmatrix} v\alpha 1 \\ v\beta 1 \\ v\alpha 3 \\ v\beta 3 \end{bmatrix} * (\frac{Ts}{VDC})$ | $V2, V3, V7, V23$ |
| $\begin{bmatrix} T1 \\ T2 \\ T3 \\ T4 \end{bmatrix} = \begin{bmatrix} -1.1180 & -0.3633 & 1.1180 & 1.5388 \\ 1.8090 & -0.5878 & 0.6910 & -0.9511 \\ -1.8090 & -0.5878 & -0.6910 & -0.9511 \\ 1.1180 & -0.3633 & -1.1180 & 1.5388 \end{bmatrix} * \begin{bmatrix} v\alpha 1 \\ v\beta 1 \\ v\alpha 3 \\ v\beta 3 \end{bmatrix} * (\frac{Ts}{VDC})$ | $V1, V3, V19, V23$ |
| $\begin{bmatrix} T1 \\ T2 \\ T3 \\ T4 \end{bmatrix} = \begin{bmatrix} -0.6910 & -0.9511 & -1.8090 & 0.5878 \\ 1.8090 & 0.5878 & 0.6910 & 0.9511 \\ -1.1180 & -1.5388 & 1.1180 & -0.3633 \\ 1.1180 & -0.3633 & -1.1180 & -1.5388 \end{bmatrix} * \begin{bmatrix} v\alpha 1 \\ v\beta 1 \\ v\alpha 3 \\ v\beta 3 \end{bmatrix} * (\frac{Ts}{VDC})$ | $V1, V17, V19, V27$ |
| $\begin{bmatrix} T1 \\ T2 \\ T3 \\ T4 \end{bmatrix} = \begin{bmatrix} 0 & -1.1756 & 0 & -1.9021 \\ 1.1180 & 1.5388 & -1.1180 & 0.3633 \\ 0 & -1.9021 & 0 & 1.1756 \\ 0.6910 & 0.9511 & 1.8090 & -0.5878 \end{bmatrix} * \begin{bmatrix} v\alpha 1 \\ v\beta 1 \\ v\alpha 3 \\ v\beta 3 \end{bmatrix} * (\frac{Ts}{VDC})$ | $V16, V17, V25, V27$ |

The simulation of the multi-dimension SVPWM besides a five-phase inverter has been done using the SABER simulation package. The results in figure 9 demonstrate the effectiveness of the multi-dimension SVPWM in generating output voltages equal to the reference signals. The reference signals are equal in magnitudes and phase-shifted by 72°.

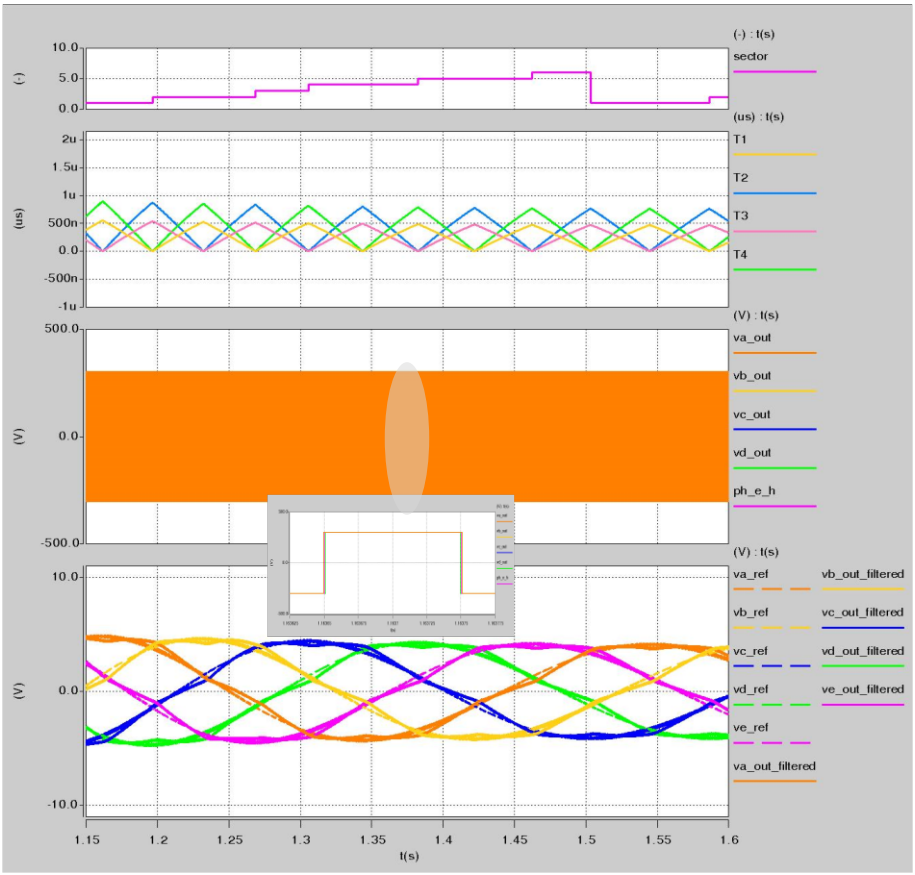


Figure 9 . simulation results obtained with multi-dimension SVPWM for healthy operating conditions

### *2.3.2 SVPWM post a failure in phase 'a'.*

To regulate the currents according to equation (18) post a failure in phase 'a', asymmetric SVPWM method can be implemented (Chen, Liu, Zhao, Qu, & Xu, 2017). This method depends on a reconstruction of the space vector diagram post the failure based on the changes of the remaining healthy currents as shown in figure 10.

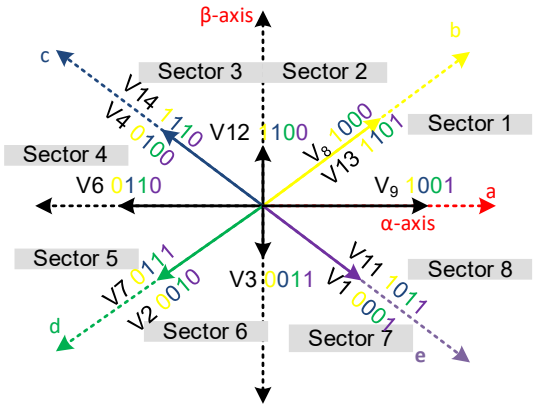


Figure 10 switching vectors on a-ß axis of asymmetric SVPWM post the failure in phase ‘a’.

The active vectors in figure 10 can be categorized into three groups according to their amplitudes. The first group contains the vectors V1, V2, V4, V7, V8, V11, V13 and V14 with amplitude equals 0.4*VDC. The second group contains the vectors V3 and V12 with amplitude equals 0.4702*VDC. Finally, the amplitudes of vectors (V6, and V9) in the third group equals 0.6472 VDC.

The algorithm to implement the SVPWM post a failure in phase ‘a’ is shown in figure 11. A fast preview of the working of each block will be presented here.

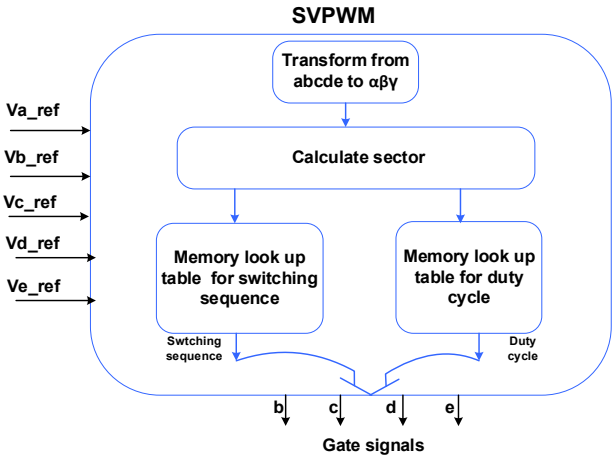


Figure 11. The algorithm of the asymmetric SPVPWM post a failure in phase ‘a’

Firstly, The reference voltage (V_ref) can be located in any of the 8 sectors according to

table 3.

Table 3. Selection of the Sector.

| Angle of reference voltage (θ) | Sector number |
|---|---|
| $0 \leq \theta < \theta_x$ | 1 |
| $\theta_x \leq \theta < 2.5\ \theta_x$ | 2 |
| $2.5\theta_x \leq \theta < 4\theta_x$ | 3 |
| $4\theta_x \leq \theta < 5\theta_x$ | 4 |
| $5\theta_x \leq \theta < 6\theta_x$ | 5 |
| $6\ \theta_x \leq \theta < 7.5\theta_x$ | 6 |
| $7.5\ \theta_x \leq \theta < 9\theta_x$ | 7 |
| $9\theta_x \leq \theta < 10\theta_x$ | 8 |

Secondly, the dwell time is calculated as shown in figure 12 and the equations below. Figure 12 illustrates how the adjacent vectors (V4=0100, V12= 1100, V14=1110 , V0=1111) are utilized to generate reference voltage (V_ref) that is located in the third sector. The duration time of the vectors V4,V12 and V0 i.e (T1/4,T2/2, and T0/4) can be deduced as follows :

$$V_1 = V_\alpha * \sin(\theta_x) - V_\beta * \cos(\theta_x) \quad (28)$$

$$T1 = \frac{-V_\alpha}{0.4*VDC*\sin(\theta_x)} * Ts \quad (29)$$

$$T2 = \frac{V_1}{0.6472*VDC*\sin(\theta_x)} * Ts \quad (30)$$

$$T0=Ts-T1-T2 \quad (31) .$$

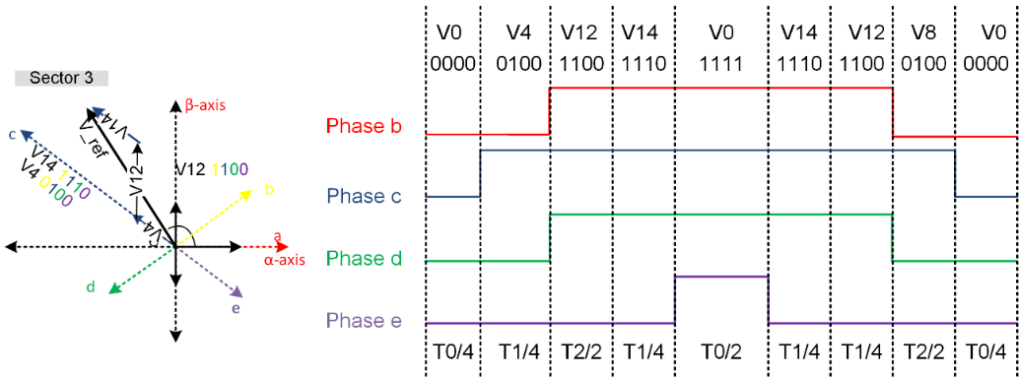


Figure 12 . illustration of the vectors and the switching sequence used to generate the reference voltage (V_ref_ α1-β1) located in the third sector using Asymmetric SVPWM.

Finally, The dwell time and the correct switching sequence in other sectors are given in table 4.

Table 4: Dwell time calculation and switching sequence in Asymmetric SVPWM

| Sector | T1 | T2 | T0 | Switching sequence |
|---|---|---|---|---|
| 1 | $\frac{V_\beta}{0.4*VDC*0.5878} * Ts$ | $\frac{V_1}{0.6472*VDC*0.5878} * Ts$ | $Ts - T1 - T2$ | $V8, V9, V13,$ |
| 2 | $\frac{V_\alpha}{0.4*VDC*0.809} * Ts$ | $\frac{-V_1}{0.4702*VDC*0.809} * Ts$ | $Ts - T1 - T2$ | $V8, V12, V13$ |
| 3 | $\frac{-V_\alpha}{0.4*VDC*0.809} * Ts$ | $\frac{V_2}{0.4702*VDC*0.809} * Ts$ | $Ts - T1 - T2$ | $V4, V12, V1$ |
| 4 | $\frac{V_\beta}{0.4*VDC*0.5877} * Ts$ | $\frac{-V_2}{0.6472*VDC*0.5877} * Ts$ | $Ts - T1 - T2$ | $V4, V6, V14$ |
| 5 | $\frac{-V_\beta}{0.4*VDC*0.5877} * Ts$ | $\frac{-V_1}{0.6472*VDC*05877} * Ts$ | $Ts - T1 - T2$ | $V2, V6, V7$ |
| 6 | $\frac{-V_\alpha}{0.4*VDC*0.809} * Ts$ | $\frac{V_1}{0.4702*VDC} * Ts$ | $Ts - T1 - T2$ | $V2, V3, V7$ |
| 7 | $\frac{V_\alpha}{0.4*VDC*0.809} * Ts$ | $\frac{-V_2}{0.4702*VDC*0.809} * Ts$ | $Ts - T1 - T2$ | $V1, V3, V11$ |
| 8 | $\frac{-V_\beta}{0.4*VDC*0.5877} * Ts$ | $\frac{V_2}{0.6472*VDC*0.5877} * Ts$ | $Ts - T1 - T2$ | $V1, V9, V11$ |

The simulation of the whole PMSM drive post a failure in phase ‘a’ using asymmetric SVPWM has been done as shown in figure 13. The results in figure 13 demonstrate the effectiveness of the asymmetric SVPWM in generating an output voltage equal to the reference signals. The reference signals ve_ref and vc_ref are shifted towards the open

circuit phase (phase ‘a’)  by 36°.

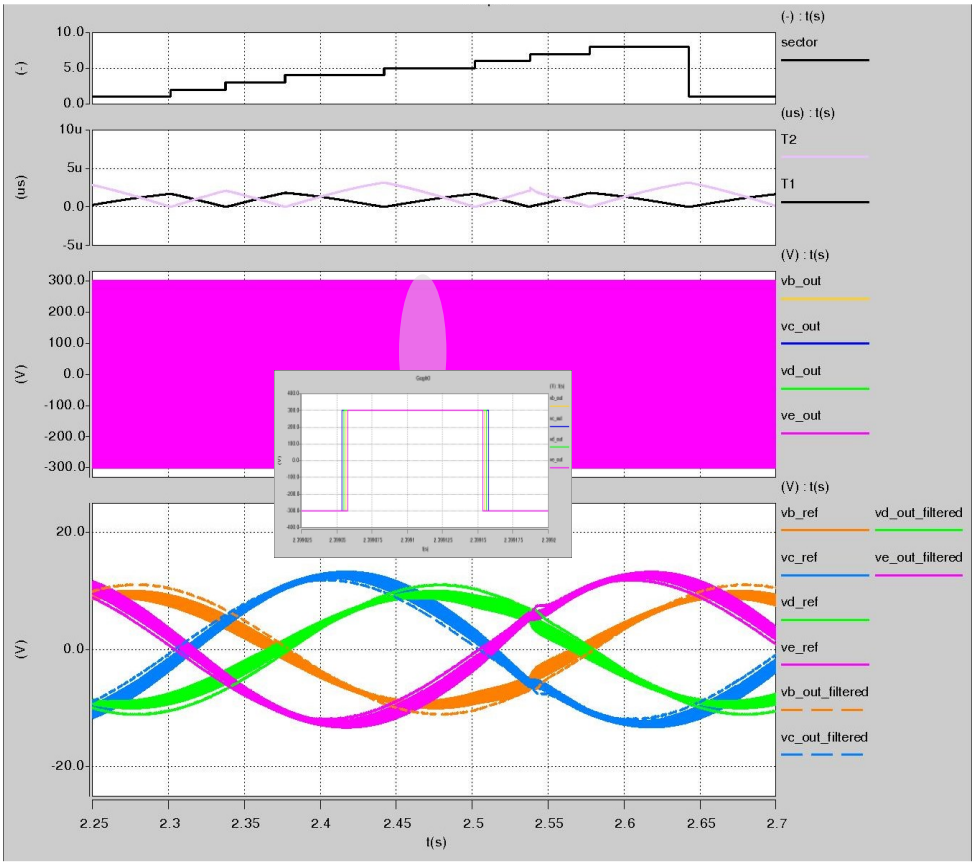


Figure 13 . simulation results obtained with asymmetrical SVPWM post a failure in phase ‘a’.

### *2.3.3 SVPWM post a failure in the adjacent phases ‘a’ and ‘b’*

To regulate the currents according to equation (20) post an open-circuit fault in the adjacent phases ‘a’ and ‘b’, a novel SVPWM method is presented in this paper. This method depends on a reconstruction of the space vector diagram post the failure  in the adjacent phases ‘a’ and ‘b’ of the five-phase motor based on the changes of the healthy remaining currents as shown in figure 14.

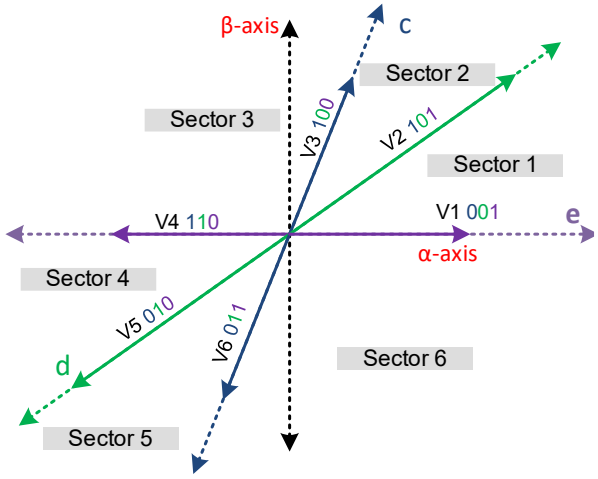


Figure 14 switching vectors on a-ß axis of a new SVPWM post a failure in adjacent phases ‘a’ and ’b’.

The vectors in figure 14 can be categorized into two groups according to their amplitudes. The first group consists of the vectors V1, V3, V4, and V6 with amplitude equals 0.4*VDC. The second group consists of the vectors V3, and V5 with amplitude equals 1.618*0.4*VDC. The amplitude of these switching vectors can be calculated directly according to the equation :-

$$Vs = \frac{2}{5} VDC \ (S_c e^{2j\theta_x} + S_d{}^{6j\theta_x} + S_e) \qquad (32)$$

Where $S_c, S_d$, and $S_e$ are the gating signals of upper switches of the phases ‘c’, ‘d’, and ‘ e’ respectively in the five phase inverter. For example if the gate pulse of leg c becomes 1 ($S_c$=1) the amplitude of the vector will be 0.4 VDC. If the gate pulses of leg c and leg e becomes one at the same time ($S_c$=$S_e$ = 1), then the amplitude of the vector will be 1.618*0.4*VDC.

The algorithm to implement the new SVPWM post a failure in the adjacent phases ‘a’ and ‘b’ is shown in figure 15. A fast preview of the working of each block will be presented here.

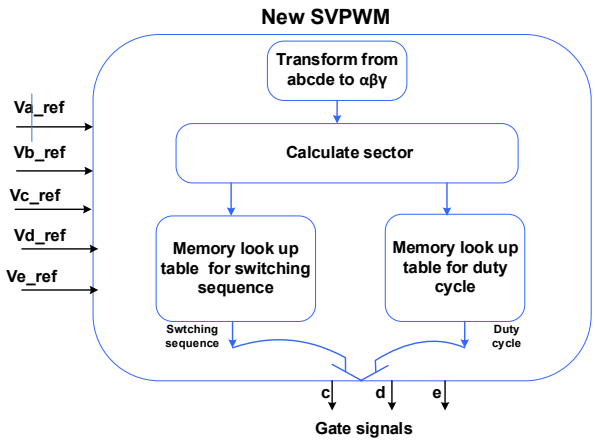


Figure 15. The algorithm of the new SPVPWM post failure adjacent phase ‘a’ and ’b’.

Firstly, The reference voltage (V_ref) can be located in any of the 6 sectors according to table 5.

Table 5. Selection of the Sector.

| Angle of reference voltage (θ) | Sector number |
|---|---|
| $0 \leq \theta < \theta_x$ | 1 |
| $\theta_x \leq \theta < 2\theta_x$ | 2 |
| $2\theta_x \leq \theta < 5\theta_x$ | 3 |
| $5\theta_x \leq \theta < 6\theta_x$ | 4 |
| $6\theta_x \leq \theta < 7\theta_x$ | 5 |
| $7\theta_x \leq \theta < 10\theta_x$ | 6 |

Secondly, the dwell time is calculated as shown in figure 16 and the equations below. Figure 16 shows how the adjacent vectors (V1=001, V2= 101, and V0=111) are utilized to generate the reference voltage (V_ref) if it is located in the first sector.

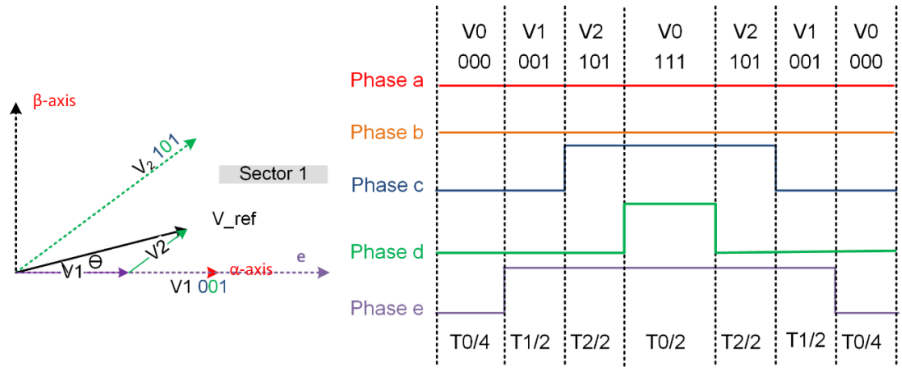


Figure 16 illustration of the vectors and the switching sequence used to generate the reference voltage located in sector 1 post a failure in adjacent phases 'a' and 'b' using the new SVPWM .

The duration of applying the vectors V1,V2 and V0 i.e (T1/4, T2/2, and T0/4) can be obtained as follows :-

$$V_\alpha * Ts = V1 * T1 + V2 * T2 * \cos\ (\theta_x) = 0.4*VDC*T1+1.618*0.4*VDC*T2* \cos\ (\theta_x) \quad (33)$$

$$V_\beta * Ts = V2 * T2 * \sin\ (\theta_x) = 1.618*0.4*VDC*T2* \sin\ (\theta_x) \quad (34)$$

From equations (33,34) the dwell time in the first sector can be calculated as shown below:-

$$T2 = \frac{V_\beta}{1.618*0.4*VDC*\sin\ (\theta_x)} * Ts \quad (35)$$

$$T2 = \frac{V_\alpha*\tan(\theta_x)-V_\beta}{0.4*VDC*\tan\ (\theta_x)} * Ts \quad (36)$$

Finally, The dwell time and the correct switching sequence in other sectors are given in table 6

Table 6: Dwell time calculation and switch sequence in new SVPWM post failure in adjacent phases 'a' and

| Sector | T1 | T2 | T0 | Switching sequence |
|---|---|---|---|---|
| 1 | $\frac{V_\alpha-1.3764*V_\beta}{0.4*VDC} * Ts$ | $\frac{1.0515*V_\beta}{0.4*VDC} * Ts$ | $Ts - T1 - T2$ | $V1, V2, V0$ |

| | | | | |
|---|---|---|---|---|
| 2 | $\frac{-V_\alpha+1.3764*V_\beta}{0.4*VDC}*Ts$ | $\frac{V_\alpha-0.3249*V_\beta}{0.4*VDC}*Ts$ | $Ts-T1-T2$ | $V3,V2,V0$ |
| 3 | $\frac{1.0515*V_\beta}{0.4*VDC}*Ts$ | $\frac{-V_\alpha+0.3249*V_\beta}{0.4*VDC}*Ts$ | $Ts-T1-T2$ | $V3,V4,V0$ |
| 4 | $\frac{-1.0515*V_\beta}{0.4*VDC}*Ts$ | $\frac{-V_\alpha+1.3764*V_\beta}{0.4*VDC}*Ts$ | $Ts-T1-T2$ | $V5,V4,V0$ |
| 5 | $\frac{-V_\alpha+1.3764*V_\beta}{0.4*VDC}*Ts$ | $\frac{V_\alpha-1.3764*V_\beta}{0.4*VDC}*Ts$ | $Ts-T1-T2$ | $V5,V6,V0$ |
| 6 | $\frac{V_\alpha-0.3249*V_\beta}{0.4*VDC}*Ts$ | $\frac{-1.0515*V_\beta}{0.4*VDC}*Ts$ | $Ts-T1-T2$ | $V1,V6,V0$ |

The simulation of the whole PMSM drive after the failure of the adjacent phases ‘a’ and ‘b’ based on the new SVPWM has been done as shown in figure 17. The results in figure 17 demonstrate the effectiveness of the new SVPWM in generating output voltages that are in phases with the reference signals. The reference signal ve_ref is shifted by 72° to replace the phase ‘a’ that is open -circuited. Also, the reference signal vc_ref shifted by 72° to replace phase ‘b’ that is open-circuited too. The difference in magnitude between the reference signal vd_ref and the output voltage of the inverter is not important. The most important thing is that the angles are equals.

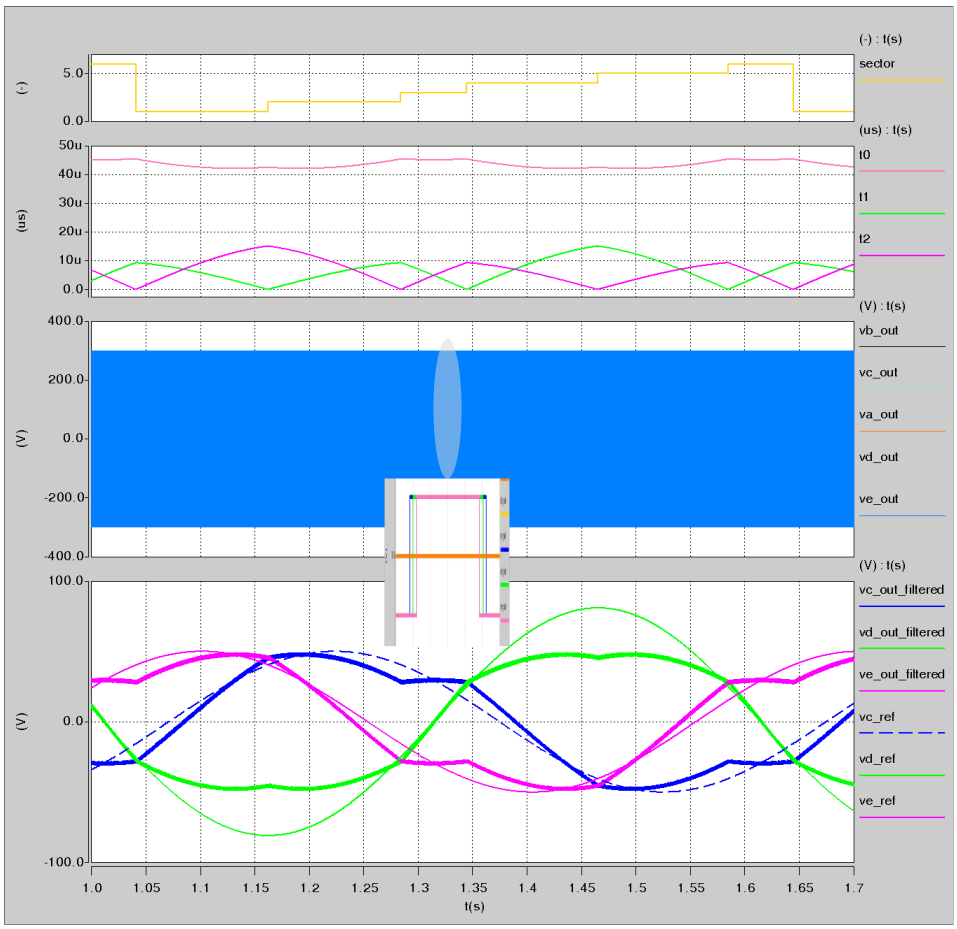

Figure 17 . simulation results obtained with new SVPWM post a failure in adjacent phases ‘a’ and ‘b’.

### *2.3.4 SVPWM post a failure in the non-adjacent phases ‘b’ and ‘e’*

To regulate the currents according to equation (20) post a failure in the non-adjacent phases ‘b’ and ‘e’, a novel SVPWM method is presented in this paper. This method depends on reconstruction of the space vector diagram post the failure in the non-adjacent phases ‘b’ and ‘e’ of the five-phase motor based on the changes in the remaining healthy currents as shown in figure 18.

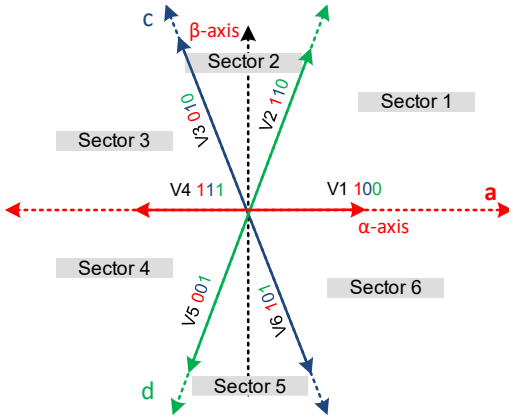


Figure 18 switching vectors on a-ß axis of a new SVPWM post a failure in the non-adjacent phases ‘b’ and’e’.

The vectors in figure 18 can be categorized into two groups according to their amplitude. The first group consists of the vectors V1, and V4 with amplitude equals 0.4*VDC. The second group consists of the vectors V2, V3, V5, and V6 with amplitude equals 1.618*0.4*VDC.

The algorithm to implement the SVPWM post a failure in the non-adjacent phases ‘b’ and ‘e’ is shown in figure 19. A fast preview of the working of each block will be presented here.

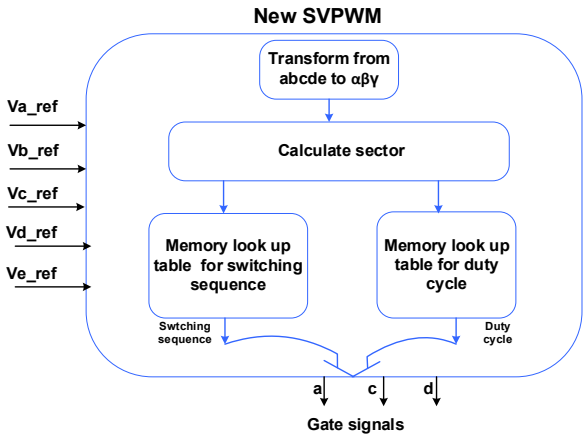


Figure 19. The algorithm of the new SPVPWM post a failure in the non-adjacent phases ‘b’ and’e’.

Firstly, The reference voltage (V_reference) can be located in any of the 6 sectors according to table 7.

Table 7. Selection of the Sector.

| Angle of reference voltage (θ) | Sector number |
|---|---|
| $0 \leq \theta < 2\theta_x$ | 1 |
| $2\theta_x \leq \theta < 3\theta_x$ | 2 |
| $3\theta_x \leq \theta < 5\theta_x$ | 3 |
| $5\theta_x \leq \theta < 7\theta_x$ | 4 |
| $7\theta_x \leq \theta < 8\theta_x$ | 5 |
| $8\theta_x \leq \theta < 10\theta_x$ | 6 |

Secondly, the dwell time is calculated as shown in figure 20 and the equations below. Figure 20 shows how the adjacent vectors (V1=100, V2= 101, and V0=111) are used to generate the reference voltage if it is located in the first sector.

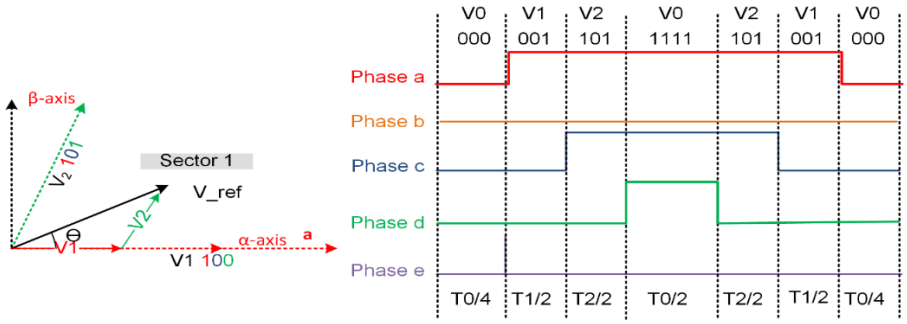


Figure 20 illustration of the vectors and the switching sequence used to generate the reference voltage vector located in sector 1 using the new SVPWM post a failure in the non-adjacent phases 'b' and 'e'.

The duration time of applying the vectors V1,V2 and V0 i.e (T1/4,T2/2 and T0/4) can be deduced as follows :-

$$V_\alpha * Ts = V1 * T1 + V2 * T2 * \cos\ (2\theta_x) = 0.4*VDC*T1+1.618*0.4*VDC*T2* \cos\ (2\theta_x) \quad (37)$$

$$V_\beta * Ts = V2 * T2 * \sin\ (2\theta_x) = 1.618*0.4*VDC*T2* \sin\ (2\theta_x) \quad (38)$$

From equations (37,38) the dwell time in the first sector can be calculated as shown below:-

$$T2 = \frac{V_\beta}{1.618*0.4*VDC*\sin\ (2\theta_x)} * Ts \quad (39)$$

$$T2 = \frac{V_\alpha*\tan(2\theta_x)-V_\beta}{0.4*VDC*\tan\ (2\theta_x)} * Ts \quad (40)$$

Finally, The dwell time and the correct switching sequence in other sectors is given in table8

Table 8: Dwell time calculation in new SVPWM in case of a failure in phases 'b' and 'e'

| Sector | T1 | T2 | T0 | Switching sequency |
|---|---|---|---|---|
| 1 | $\frac{V_\alpha-0.325*V_\beta}{0.4*VDC} * Ts$ | $\frac{0.65*V_\beta}{0.4*VDC} * Ts$ | $Ts - T1 - T2$ | $V1, V2, V0$ |

| | | | | |
|---|---|---|---|---|
| 2 | $\frac{-V_\alpha+0.325*V_\beta}{0.4*VDC}*Ts$ | $\frac{V_\alpha+0.325*V_\beta}{0.4*VDC}*Ts$ | $Ts-T1-T2$ | $V3,V2,V0$ |
| 3 | $\frac{0.65*V_\beta}{0.4*VDC}*Ts$ | $\frac{-V_\alpha-0.325*V_\beta}{0.4*VDC}*Ts$ | $Ts-T1-T2$ | $V3,V4,V0$ |
| 4 | $\frac{-0.65*V_\beta}{0.4*VDC}*Ts$ | $\frac{-V_\alpha+0.325*V_\beta}{0.4*VDC}*Ts$ | $Ts-T1-T2$ | $V5,V4,V0$ |
| 5 | $\frac{-V_\alpha-0.325*V_\beta}{0.4*VDC}*Ts$ | $\frac{V_\alpha-0.325*V_\beta}{0.4*VDC}*Ts$ | $Ts-T1-T2$ | $V5,V6,V0$ |
| 6 | $\frac{V_\alpha+0.325*V_\beta}{0.4*VDC}*Ts$ | $\frac{-0.65*V_\beta}{0.4*VDC}*Ts$ | $Ts-T1-T2$ | $V1,V6,V0$ |

The simulation of the whole PMSM drive post an open-circuit fault in a non-adjacent phase ‘b’ and ‘e’ base on the new SVPWM has been done as shown in figure 21. The results in figure 21 demonstrate the effectiveness of the new SVPWM in generating the output voltage that are in phases with the reference signals. The reference signal vc_ref is shifted by 36° in the direction of the open circuit phase ‘b’. Also, the reference signal vd_ref is shifted by 36° in the direction of the open circuit phase ‘e’. The difference in magnitude between the reference signals vd_ref, and vc_ref and the output voltage of the inverter is not important. The most important thing is that the angles are equals.

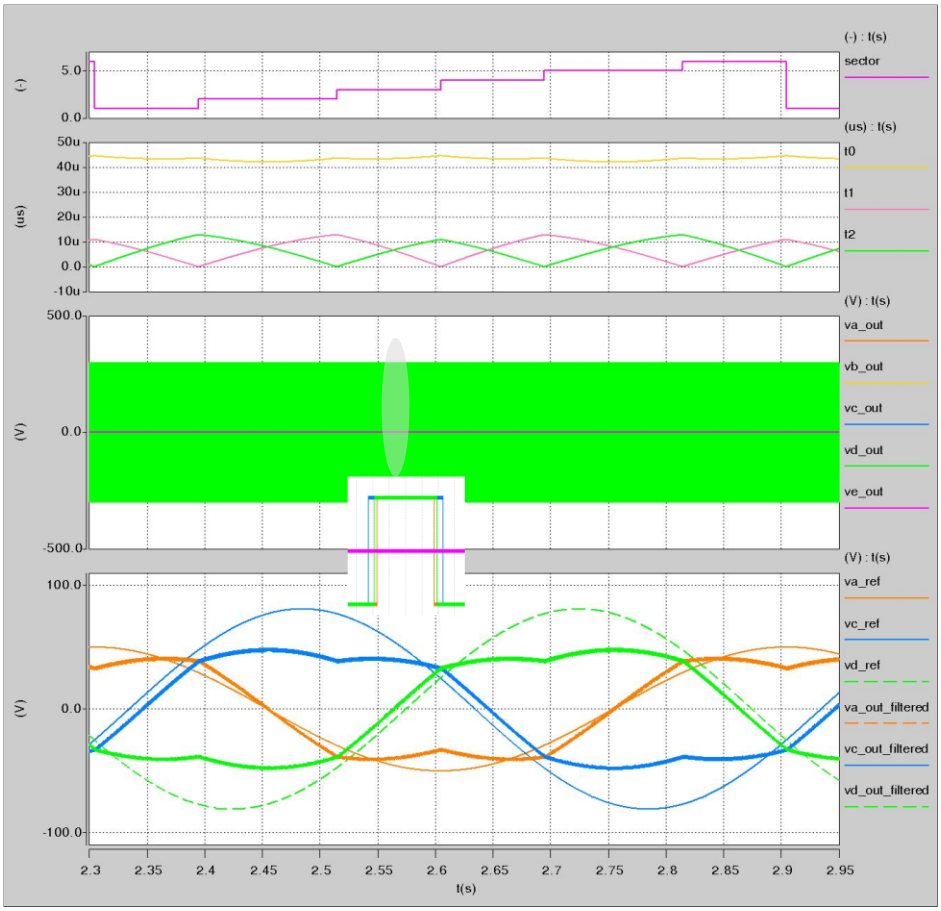


Figure 21 . simulation results obtained with new SVPWM post a failure in the non-adjacent phases ‘b’ and ‘e’.

### *2.3 Simulation results of the Fault -Tolerant PMSM Drive*

The multi-dimension SVPWM, asymmetric SVPWM, in addition to the new SVPWM techniques proposed in this paper has been simulated in the SABER simulation platform as shown in figure 22. Multi-dimension SVPWM will be adopted in the case that the motor is not running without any fault. If a single-phase open-circuit fault is introduced to phase ‘a’, the asymmetric SVPWM technique will be adopted. The two new SVPWM techniques illustrated in section 2.3.3 and 2.3.4 will be adopted if the open-circuit fault was introduced to two adjacent phases ‘a’ and ‘b’ and a two non-adjacent phase ‘b’ and ‘e’ respectively

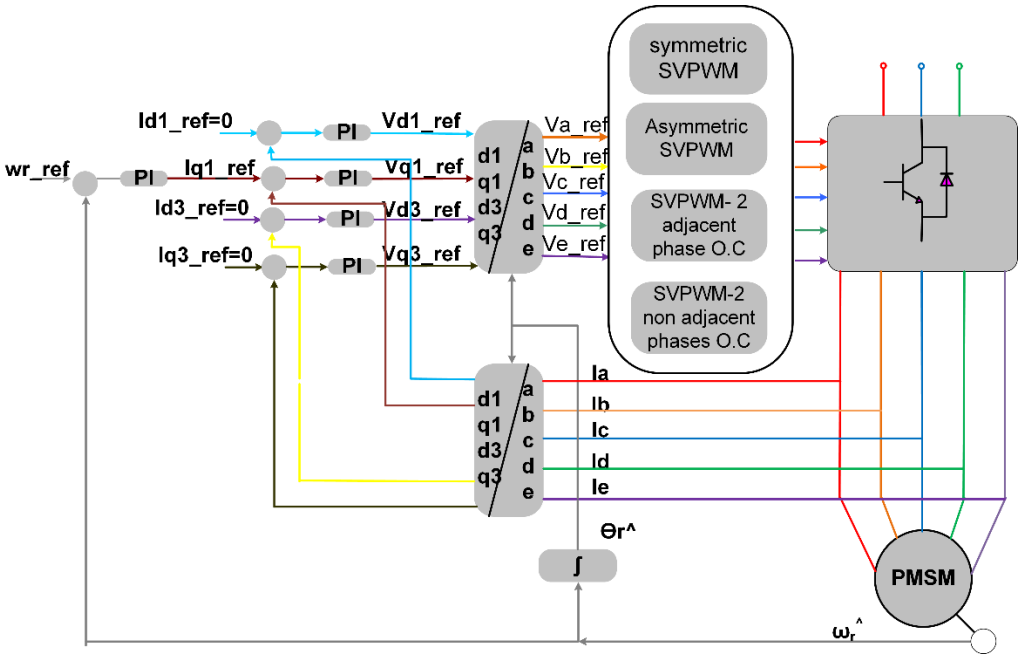


Figure 22 FOC control structure for a fault-tolerant five phase drive.

The simulation results obtained from implementing the FOC scheme illustrated in figure 22 are shown in figure 23. The motor was running at 250 rpm and full load and the multi-dimension SVPWM was used. The stator currents in this period are equal in magnitude and phase-shifted by 72° similar to those given in equation (15) . Then at time t=2 s, a failure happened in phase ‘a’ at the same time the asymmetric SVPWM was utilized. The remaining stator currents in this period reaches 138.2% of the stator current under healthy condition. Moreover, the currents ‘ib’ and ‘ie’ were shifted by 36° towards the failure phase ‘a’. These results are similar to those obtained in equation (18). From t=2.5s to t=3s, the motor returned to work as before the fault. At t=3s, failure in the adjacent phases ‘a’ and ‘b’ occurred and at the same time, the new modulation technique presented in section 2.3.3 was implanted. Many observations can be mentioned based on the results. Firstly: the current in phase ‘d’ reached 361.8% of its value under healthy operating conditions. Secondly: the current in phases ‘c’ and ‘e’ area also increased and reach 223.6% their values under healthy operating conditions. Finally, the currents in phase ‘c’ is shifted by 72° to replace the failure phase ‘b’ while the current in phase ‘e’ is

shifted by 72° towards the failure phase ‘a’. These observations are the same as the current equations given in equation (20). After that, at t=3.5s, the failure was removed from phase ‘a’ and phase ’b’ and the motor returned to run under healthy operating conditions, and the currents returned to the normal situation. Finally, at t=4s, the non-adjacent phases ‘b’ and ‘e’ were exposed to a failure and at the same time, the new modulation technique presented in section 2.3.4 was implanted. Many points can be noticed from the current waveforms in this interval. Firstly: the current in phase ‘a’ reached 138.2% of its value under healthy operating conditions. Secondly: the current in phases ‘c’ and ‘d’ are also increased and reach 223.6% of their values under healthy operating condition. Finally, the current in phase ‘c’ is shifted by 36° towards the failure phase ‘b’ while the current in phase ‘d’ is shifted by 36° towards the failure phase ‘e’. These observations are the same as the current equations given in equation (22). The most important thing that can be demonstrated from the result is that the ripple in speed and torque was minimum and almost negligible even at extreme cases when the two phases of the motor were exposed to failure. Moreover, a Fast Fourier Transform (FFT) was done to the current in phase ‘c’ under healthy operating condition, fault in phase ‘a’, fault in adjacent phases ‘a’ and ’b’, and fault in nonadjacent phases ‘b’ and ‘e’ to check whether the new modulation techniques proposed in sections 2.3.3 and 2.3.4 affect the power quality by generating extra harmonics in the motor healthy currents post the fault. The FFT shows a slightly increase in third harmonics using the new modulation techniques which will not affect the THD. The FFT also proves that no extra harmonics are generated using the new modulation techniques.

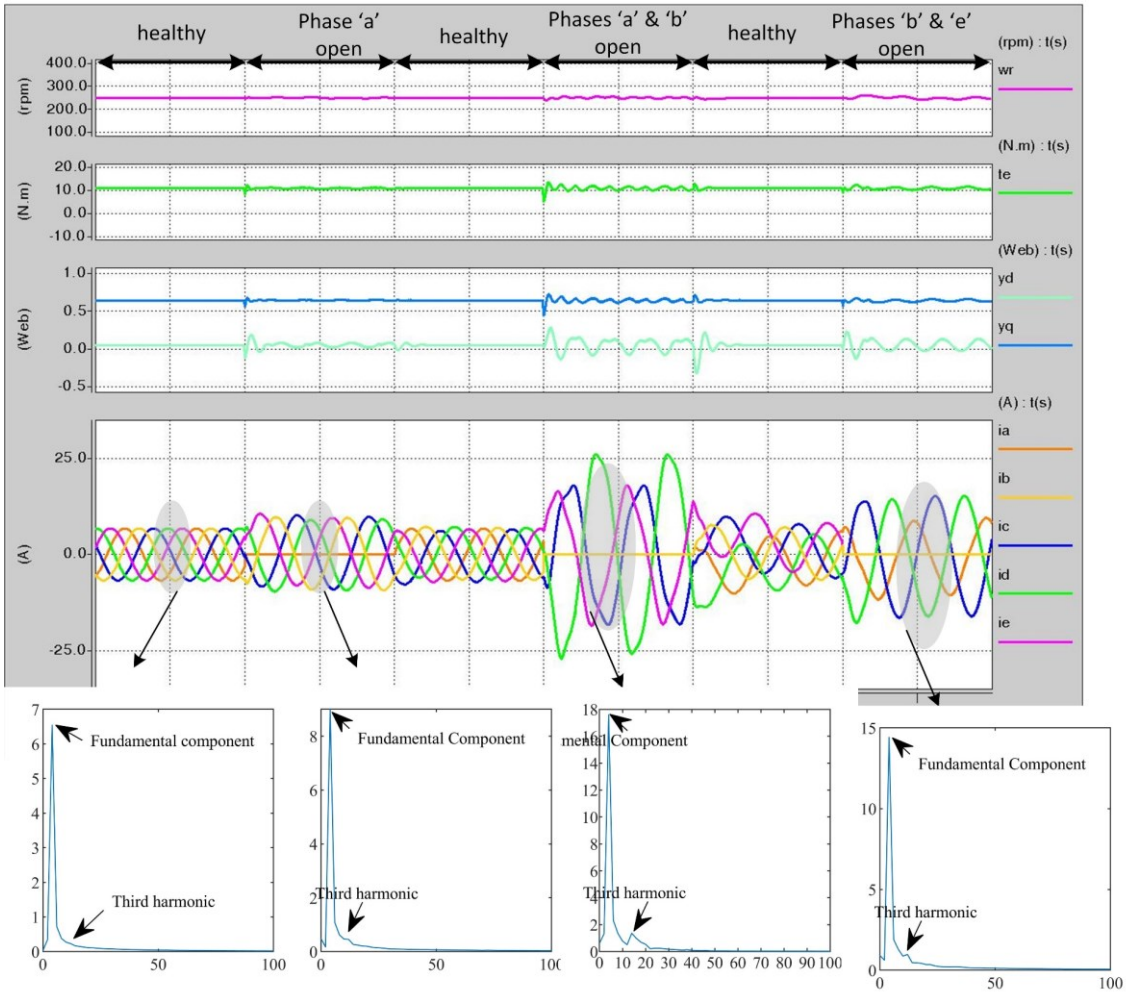


Figure 23: simulation results of the five-phase motor drive under different fault conditions.

Figure 24 demonstrates the results obtained from a five-phase motor runs under speed control at 50% load pre and post a failure in the adjacent phases 'a' and 'b' and the nonadjacent phases using the new modulation techniques proposed in sections 2.3.3 and 2.3.4. The motor was running at speed = 200 rpm using the multi-dimension SVPWM without any fault. At t=2s, a failure in the adjacent phases 'a' and 'b' occurred and at the same time the new modulation technique proposed in section 2.3.3 was used. Then at t=2.5 s and while the adjacent phases 'a' and 'b' are still failure, the reference speed of the motor was set to 0 rpm. Figure 24 shows that the motor real speed became 0 rpm in less than 1 second. After that, at t=4s, and while the motor is at zero speed, the motor

returned to run under healthy operating conditions. At time t = 6s, a failure in the non adjacent phases ‘b’ and ‘e’ happened and at the same time the new modulation technique proposed in section 2.3.4 was used. Finally, at t=6.5 s, the reference speed of the motors was set to -200 rpm . Figure 24 shows that performance of the whole system post the failure in the two phases is as good as the performance in healthy mode.

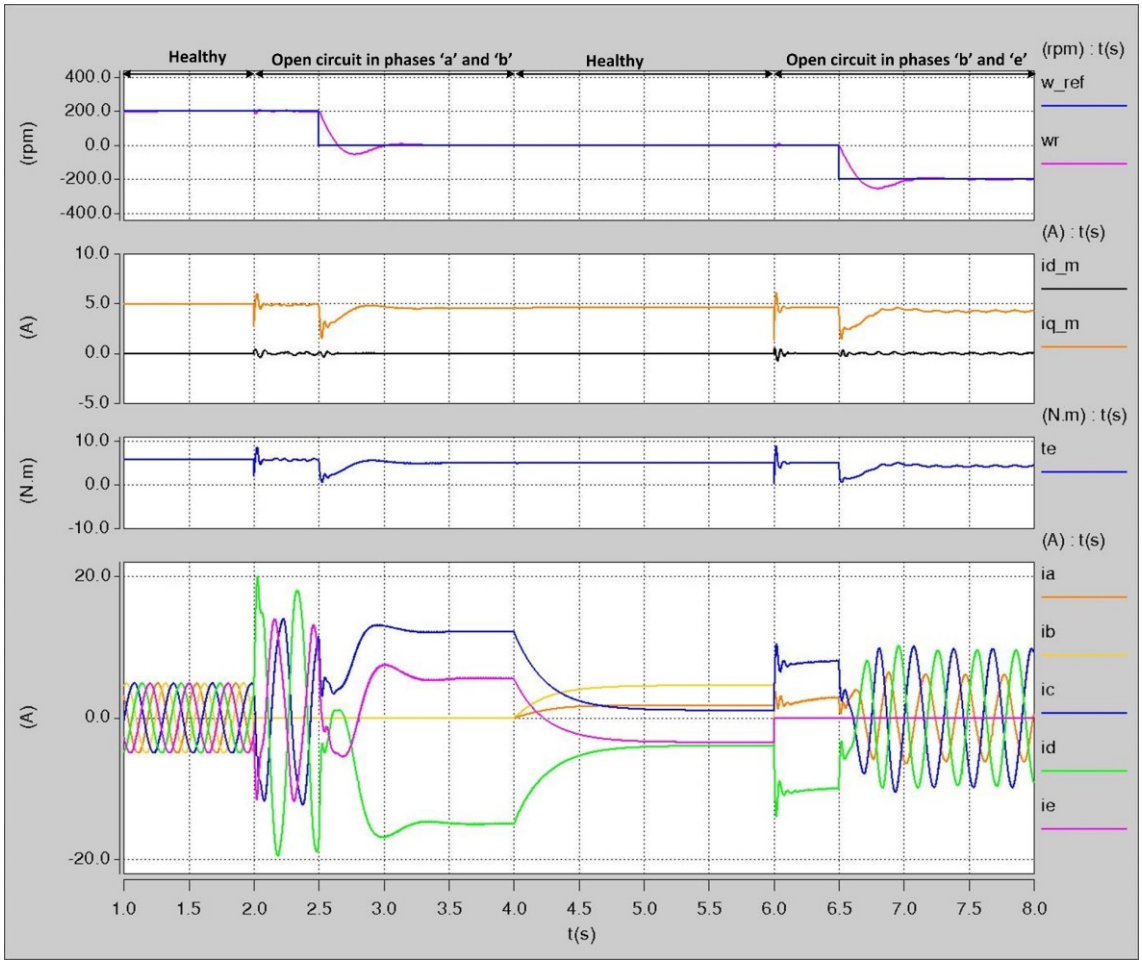


Figure 24: simulation results for low speed steps of a fault-tolerant five-phase motor drive post a failure in the adjacent phases ’a’and ’b’ and non adjacent phases ‘b’ and ‘e’ using the new SVPWM proposed in sections 2.3.3 and 2.3.4 .

Figure 25 demonstrates the results obtained from a five-phase motor runs under speed control at 50% load pre and post failure in the non-adjacent phases ‘b’ and ‘e’ using the new modulation technique proposed in section 2.3.4. The motor was running at speed =200 rpm without any fault and the multi-dimension SVPWM was utilized. At t=2s, a

failure in the non-adjacent phases ‘b’ and ‘e’ occurred and the same time the new modulation technique proposed in section 2.3.4 was utilized. Then at t=2.5 s and while the phases ’b’ and ‘e’ are a failure, the reference speed of the motor was set to 0 rpm. Figure 25 shows that the motor real speed became 0 rpm in less than 1 second. After that, at t=4s, and while the motor is still at zero speed, the motor returns to run under healthy operating conditions. At time t = 6s, a failure in the non-adjacent phases ‘b’ and ‘e’ happened. Finally, at t=6.5 s, the reference speed of the motor was set to 200 rpm while the non-adjacent phases ‘b’ and ‘e’ are failure. Figure 25 shows that performance of the whole system post the failure fault in the non-adjacent phases ‘b’ and ‘e’ is as good as it is in healthy mode.

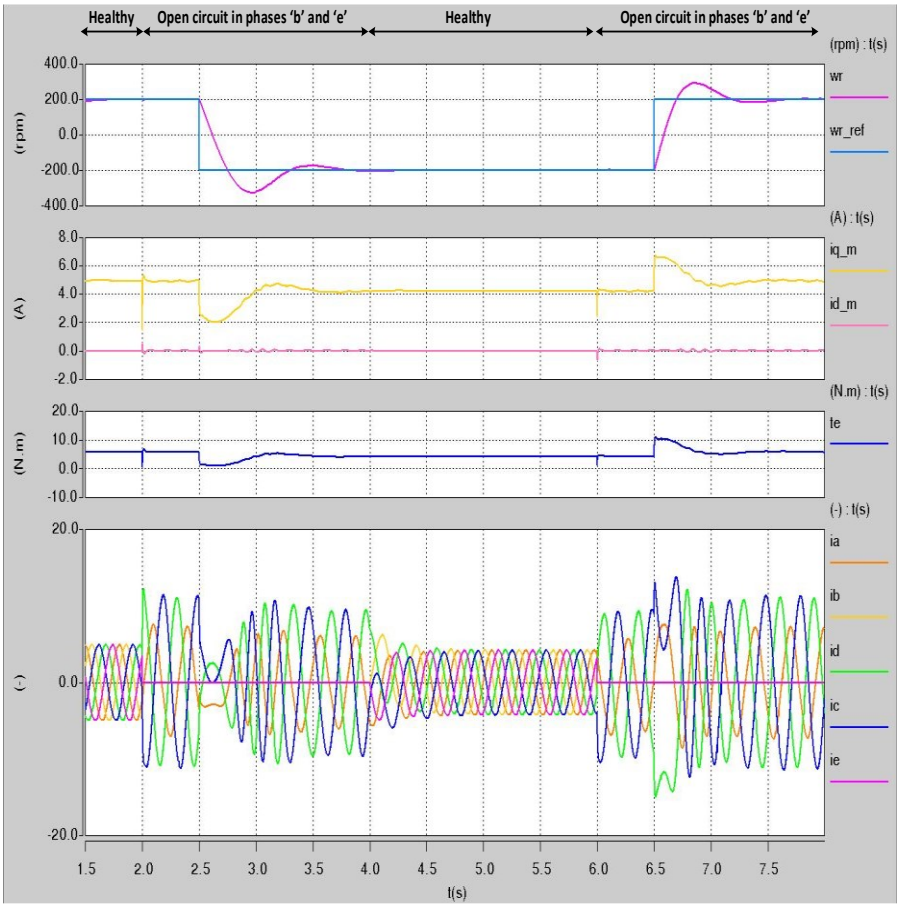


Figure 25: simulation results for low speed steps of a fault-tolerant five-phase motor drive post a failure in the non-adjacent phases ’b’ and ’e’ using the new SVPWM proposed in section 2.3.4.

Figure 26 illustrates the stability of the drive system at low speed (200 rpm) and under two phase failures when a load disturbance is applied. The results show that the system maintains the speed in all the cases.

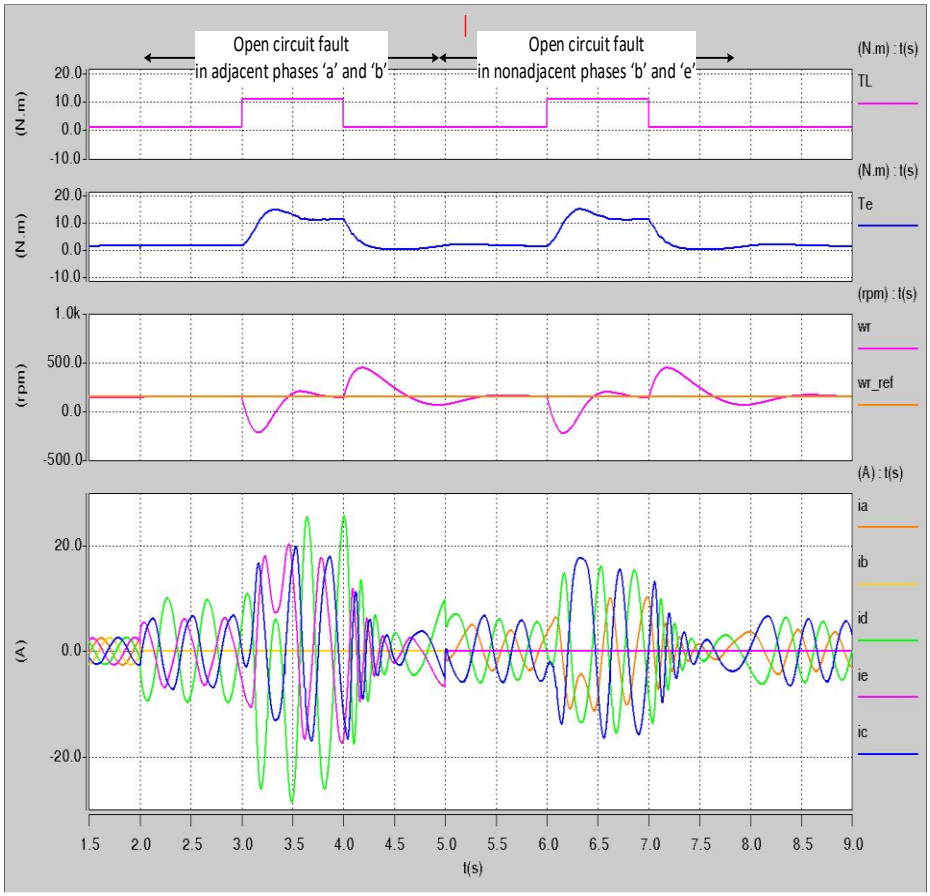


Figure 26: simulation results for load steps under failure in the adjacent phases 'a' and 'b' and the non-adjacent phases 'b' and 'e'.

## 3. Conclusion

This paper has proposed two new SVPWM techniques SVPWM used in a five-phase motor drive system post a failure in the adjacent phases 'a' and 'b' and the non-adjacent phases 'b' and 'e' as shown in section 2.3.3 and 2.3.4 respectively. The new SPWM techniques are based on the changes in magnitudes and currents under the failure. The new algorithms can be used for five permanent-magnet drives and five- phase induction motor drive. Comapred to other FTC of the five phase motor, the new technique is simple to implement in hardware and need no extra memory. Also it is using FOC control which widely used in industry. Most

importantly, it very suitable to be implemented in the cases when the sensorless control of the five phase motor using the fundamental PWM excitation method under the two phases failure is wanted which will be the next step in this research. Simulation results illustrate the capability of proposed new SVPWM techniques to maintain the operation of the five-phase motor post a two-phase failure. In addition to maintain the torque ripple less than 3.6 % and 3.4% post the failure in adjacent phase and non-adjacent phases respectively.

References


Villani, M., Tursini, M., Fabri, G. & Castellini, L. (2010, December). Multi-phase fault tolerant drives for aircraft applications. In Electrical Systems for Aircraft, Railway and Ship Propulsion conference (pp. 1-6). Bologna, Italy.

Qingguo, S., Xiaofeng, Z., Fei, Y. & Chengsheng, Z. (2005, September). Research on Space Vector PWM of Five-Phase Three-Level Inverter. In International Conference on Electrical Machines and Systems (pp. 1418-1421). Nanjing, China.

Chen, K. (2015, June ). Multiphase pulse-width modulation considering reference order for sinusoidal wave production. In IEEE 10th Conference on Industrial Electronics and Applications (ICIEA) (pp. 1155-1160). Auckland, New Zealand,.

Xue, S., Wen, X., & Feng, Z. (2006, August). A Novel Multi-Dimensional SVPWM Strategy of Multiphase Motor Drives. In 12th International Power Electronics and Motion Control Conference (pp. 931-935). Shanghai, China .

Wang, P., Zheng., P., Wu, F., Zhang, J. & Li, T. (2014, August). Research on dual-plane vector control of fivephase fault-tolerant permanent magnet machine. in IEEE Conference and Expo Transportation Electrification Asia-Pacific (ITEC Asia-Pacific) (pp. 1-5). Beijing, China.

Parsa, L. & Toliyat, H. (2007). Sensorless Direct Torque Control of Five-Phase Interior Permanent-Magnet Motor Drives. IEEE Transactions on Industry Applications. 43, 4, pp. 952-959.

Bianchi, N., Bolognani, S. & Dai Pre, M. (2007). Strategies for the Fault-Tolerant Current Control of a Five-Phase Permanent-Magnet Motor. IEEE Transactions on Industry Applications. 43,4, pp. 960-970.

Mohammadpour, A., Sadeghi, S., & Parsa, L. (2014). A Generalized Fault-Tolerant Control Strategy for Five-Phase PM Motor Drives Considering Star, Pentagon,

and Pentacle Connections of Stator Windings. *Industrial Electronics, IEEE Transactions on.* 61, pp. 63-75.

Abdel-Khalik, A., Ahmed, S., Elserougi, A., & Massoud, A. (2015). Effect of Stator Winding Connection of Five-Phase Induction Machines on Torque Ripples Under Open Line Condition. Mechatronics, IEEE/ASME Transactions on. 20, pp. 580-593.

Sedrine, E., Ojeda, J., Gabsi, M., & Slama-Belkhodja, I. (2015). Fault-Tolerant Control Using the GA Optimization Considering the Reluctance Torque of a Five-Phase Flux Switching Machine. in IEEE Transactions on Energy Conversion, 30, 3, pp. 927-938.

Liu, G., Qu, L., Zhao, W., Chen, Q., & Xie, Y. (2016). Comparison of Two SVPWM Control Strategies of Five-Phase Fault-Tolerant Permanent-Magnet Motor. In IEEE Transactions on Power Electronics, 31, 9, pp. 6621-6630.

Chen, Q., Liu, G., Zhao, W., Qu, L. & Xu, G. (2017). Asymmetrical SVPWM Fault-Tolerant Control of Five-Phase PM Brushless Motors. *IEEE Transactions on Energy Conversion*. 32, 1, pp. 12-22.

Guzman, H., Duran, M., Barrero, F., Zarri, L., Bogado, B., Prieto, I. & Arahal, M. (2016). Comparative study of predictive and resonant controllers in fault-tolerant five-phase induction motor drives. IEEE Transactions on Industrial Electronics. 63, 1, pp. 606–617.

Cheng, L., Sui, Y., Zheng, P., Wang, P., & Wu, F. (2018). Implementation of postfault decoupling vector control and mitigation of current ripple for five-phase fault-tolerant PM machine under single-phase open-circuit fault. IEEE Trans. Power Electron., 33, 10, pp. 8623–8636.

Zhou, H., Zhao, W., Liu, G., Cheng, R., & Xie, Y. (2017). Remedial field-oriented control of five-phase fault-tolerant permanent-magnet motor by using reduced-order transformation matrices. In IEEE Trans. Ind. Electron., 64, 1, pp. 169–178.

Chen, Q., Zhao, W., Liu, G., & Lin, Z. (2019). Extension of virtual-signal injection-based MTPA control for five-phase IPMSM into fault-tolerant operation. In IEEE Trans. Ind. Electron., 66, 2, pp. 944–955.

Chen, Q., Gu, L., Lin, Z., & Liu, G. (2020). Extension of space-vector signal-injection-based MTPA control into SVPWM fault-tolerant operation for five-phase IPMSM. In IEEE Trans. Ind. Electron., 67, 9, pp. 7321–7333.

Tian, B., An, Q., Duan, J., Semenov, D., Sun, D., & Sun, L. (2017). Cancellation of torque ripples with FOC strategy under two-phase failures of the five-phase PM motor. In IEEE Trans. Power Electron., 32, 7, pp. 5459–5472.

Liu, G., Lin, Z., Zhao, W., Chen, Q., & Xu,G. (2018). Third harmonic current injection in fault-tolerant five-phase permanent-magnet motor drive. In IEEE Trans. Power Electron., 33, 8, pp. 6970–6979.

Xiong, C., Guan, T., Zhou, P., & Xu, H. (2020). A fault-tolerant FOC strategy for five-phase SPMSM with minimum torque ripples in the full torque operation range under double-phase open-circuit fault. In IEEE Trans. Ind. Electron., 67, 11, pp. 9059–9072.

Bermudez, M., Gonzalez-Prieto, I., Barrero, F., Guzman, H., Kestelyn, X., & Duran, m. (2018). An Experimental Assessment of Open-Phase Fault-Tolerant Virtual-Vector-Based Direct Torque Control in Five-Phase Induction Motor Drives. In IEEE Transactions on Power Electronics, 33, 3, pp. 2774-2784.

Tian, B., Mirzaeva, G., An, Q., Sun, L., & Semenov, D. (2018). Fault-Tolerant Control of a Five-Phase Permanent Magnet Synchronous Motor for Industry Applications. In IEEE Transactions on Industry Applications, 54, 4, pp. 3943-3952.

Huang, W., Hua, W., Chen, F., Yin, F., & Qi, J. (2018). Model Predictive Current Control of Open-Circuit Fault-Tolerant Five-Phase Flux-Switching Permanent Magnet Motor Drives. In IEEE Journal of Emerging and Selected Topics in Power Electronics,6,4, pp. 1840-1849.

Priestley, M., Farshadnia, M., & Fletcher, J. (2019). FOC Transformation for Single Open-Phase Faults in the Five-Phase Open-End Winding Topology. IEEE Transactions on Industrial Electronics, pp. 1-1, 2019.

Tian, B., An, Q., Duan, J. , Sun, D., Sun, L., & Semenov, D. (2019). Decoupled Modeling and Nonlinear Speed Control for Five-Phase PM Motor Under Single-Phase Open Fault. In IEEE Transactions on Power Electronics, 32, 7, pp. 5473-5486.

Hyung-Min, R., Ji-Woong, K. & Seung-Ki, S. (2004, October). Synchronous frame current control of multi-phase synchronous motor - part ii asymmetric fault condition due to open phases. in Industry Applications Conference of 39th IAS Annual Meeting(p. 275). Seattle,USA.

Fu, J.R & Lipo T.A. (1994). Disturbance-free operation of a multiphase current-regulated motor drive with an opened phase. IEEE Trans. Ind. Appl. 30, 5, pp. 1267– 1274.

Zhang, W., Xu, D., Enjeti, P., Li, H., Hawke, J. & Krishnamoorthy, H. (2014). Survey on Fault-Tolerant Techniques for Power Electronic Converters. Power Electronics, IEEE Transactions on. 29, 12, pp.6319,6331.

Tani, A., Mengoni, M., Zarri, L., Serra G. & Casadei, D. (2012). Control of multi-phase induction motors with an odd number of phases under open circuit faults. IEEE Trans. Power Electron.27, 2, pp. 565–577.